Int. J. Electrochem. Sci., 15 **(2020)** 5945 – 5955, doi: 10.20964/2020.07.60

International Journal of
ELECTROCHEMICAL
SCIENCE
www.electrochemsci.org

Nickel Hexacyanoferrate Derived β-$Ni(OH)_2$ Flakes as Electrochemical Sensor for Sensitive Detection of Hydrazine

Li Zheng[*], *Chao-Rui Zhang*[a], *Dan Zhao*[a], *Xuan Wang*[a], *Ting-Ting Du*

College of Chemistry and Chemical Engineering, Xi'an Shiyou University, Xi'an, 710065, PR China
[*]E-mail: lzheng@xsyu.edu.cn
[a]These authors have the same contributions to the work

Received: 31 March 2020 / *Accepted:* 5 May 2020 / *Published:* 10 June 2020

A β-$Ni(OH)_2$ flakes modified carbon paste electrode [$Ni(OH)_2$/CPE] has fabricated for hydrazine sensing. The β-$Ni(OH)_2$ flakes derived from nickel hexacyanoferrate (NiHCF) through a facile in situ electrochemical method and characterized by Fourier transform infrared spectrometry, X-ray diffraction, and scanning electron microscopy. Meanwhile, the electrochemical performances of the modified electrode studied by electrochemical impedance spectroscopy, chronocoulometry, cyclic voltammetry, and linear sweep voltammetry. Owing to the large active surface area and enhanced electron transfer efficiency of β-$Ni(OH)_2$ flakes, the $Ni(OH)_2$/CPE showed enhanced catalytic activity toward the oxidation of hydrazine compared with NiHCF/CPE and unmodified CPE. Under the optimized conditions, the amperometric current presented linear dependence on the concentration of hydrazine in the ranges of 0.1 ~ 600 μM with the detection limit of 0.04 μM. Furthermore, the sensor has applied for the determination of hydrazine in water samples.

Keywords: Nickel hydroxide flakes; nickel hexacyanoferrate, hydrazine; electrocatalysis; electrochemical sensors

1. INTRODUCTION

Hydrazine is a strong reductant and an important industrial material, widely used in rocket propellants, fuel cells, explosives, metal film manufactures, insecticides, and photographic chemicals [1]. However, hydrazine is very toxic. It can irritate the eyes, absorb via the skin, and strongly injure the skin and mucous membrane, damage the liver and kidney, interfere with blood production and even cause cancer [2, 3]. Therefore, the quantification of hydrazine is of importance. Many methods as chromatography [4], fluorometry [5], chemiluminescence [6], and voltammetry [7] have developed to determine the hydrazine. Among them, voltammetry is more advantageous because of its high sensitivity, good selectivity, rapid response, and low cost. Various catalytic materials such as metal and metal oxide

[8-10], polymers [11-13] and complexes [14-16] have modified on the electrode surface to enhance the response current and to reduce the over-potential for the oxidation of hydrazine. However, novel materials with high catalytic activity and low cost for sensitive hydrazine quantification are still needed.

It knows that nickel is an earth-abundant transition metal. Nickel-based materials have widely applied in many fields, such as rechargeable batteries [17, 18], supercapacitors [19, 20], electro-catalysis [21, 22], and electrochemical sensors [23-25]. Among them, nickel hydroxide as an efficient catalyst has extensively studied. Different morphologies of nickel hydroxide have prepared to improve its performance. For example, nickel hydroxide nanosphere [26], nanorod [27], nanosheets [28], nanoflowers [29] for supercapacitors, nanoflake [30] for lithium-ion batteries, nanoporous nickel hydroxide for water splitting [31], nanoribbons for electro-oxidation of urea [32], nano petals for montelukast sensor [33], and nanoplates for hydrazine sensors [34, 35]. Ji et al. synthesized β-nickel hydroxide nanoplates on Cu rods by a hydrothermal method without the use of surfactants and got a detection limit of 0.3 μM for hydrazine [34]. Avanes et al. synthesized β-nickel hydroxide nanoplatelets by a hydrothermal method to modify a carbon paste electrode and got a detection limit of 0.28 μM for hydrazine [35]. Prathap et al. synthesized $Ni(OH)_2$–MnO_2 hybrid nanostructures by surfactant-free hydrothermal method, and got a low detection limit of 0.12 μM for hydrazine [36]. To our knowledge, there is no report about hydrazine sensor on nickel hexacyanoferrate derived nickel hydroxide flakes.

In the present work, a $Ni(OH)_2$ modified carbon paste electrode $Ni(OH)_2$/CPE has fabricated. The hierarchically β-$Ni(OH)_2$ flakes synthesized from nickel hexacyanoferrate (NiHCF) nanocubes by in-situ electrochemical method. The prepared sensor obtained a low detection limit of 0.04 μM for hydrazine, and had good selectivity and stability.

2. EXPERIMENTAL

2.1. Materials

Hydrazine hydrochloride ($N_2H_4 \cdot 2HCl$), nickel (II) sulfate hexahydrate ($NiSO_4 \cdot 6H_2O$), potassium hexacyanoferrate [$K_3Fe(CN)_6$], citrate sodium ($Na_3C_6H_5O_7 \cdot 2H_2O$), anhydrous alcohol ($C_2H_5OH$), sodium hydroxide (NaOH), potassium chloride, magnesium chloride, calcium acetate, ammonium carbonate, ferrous chloride, zinc sulfate, paraffin oil, and graphite powder supply by Aladdin Chemical Reagents Company (Shanghai, China) and of analytical pure. The experimental water is twice-distil.

2.2. Apparatus

The electrochemical measurement carries out on the 660A electrochemical analyzer (CHI, China). The working electrode, reference electrode, and counter electrode are a $Ni(OH)_2$/CPE, a saturated calomel electrode (SCE), and a platinum plate, respectively. Cyclic voltammetry (CV) scans in the potential range of 0.0 to 0.8 V. The electrochemical impedance spectroscopy (EIS) records in the frequency from 0.1 Hz to 100.0 kHz. The chronocoulometry performs with a single step and the pulse width of 0.25 s. Scanning electron micrographs (SEM) records by an EM-30 plus microscope (COXEM, South Korea). X-ray diffraction (XRD) patterns conduct by a D8 X-ray polycrystalline diffractometer

(Bruker, Germany). Fourier transforms infrared (FTIR) spectrograms measures by a Nicolet 5700 FTIR spectrometer (Thermo, America).

2.3. Preparation of nickel hexacyanoferrate (NiHCF) and β-Ni(OH)$_2$

The NiHCF framework prepared by a chemical precipitation method [37]. 1.32 g $K_3Fe(CN)_6$ was dissolved in 100 mL H_2O to form solution A, 1.58 g $NiSO_4 \cdot 6H_2O$ and 3.3 g sodium citrate were dissolved in 100 mL H_2O to form solution B. Solution B dropped into solution A and kept stirring for 1 hour. Then the generated yellow precipitate stood for 24 hours, separated by centrifugation, and washed with water and absolute ethanol respectively, dried in a vacuum drying oven at 60 ℃ for 8 hours, and obtained the NiHCF precursor.

CPE prepared as follows. 1.0 g graphite powder and 0.25 g paraffin oil mixed well in a 25 mL beaker. A part of the obtained pastes tightly filled into the cavity of a 3 mm diameter plastic tube, and a copper wire used as the conducting wire. Then the electrode surface polished on a tracing paper and flushed with water.

The $Ni(OH)_2$/CPE was prepared by in situ electrochemical methods. 10 mg NiHCF dispersed homogeneously in 100 mL water to form a 0.1 mg/mL solution. 3 μL of the above solution dropped onto the surface of CPE, dried it in an infrared lamp, and formed the NiHCF/CPE. Then the NiHCF/CPE was set into 1 M NaOH solution, scanned for 45 cycles in the potential range of 0 ~ 0.8 V with a scan rate of 0.1 Vs^{-1}, washed with water carefully, and obtained the $Ni(OH)_2$/CPE.

3. RESULTS AND DISCUSSION

3.1. Preparation of nickel hydroxide

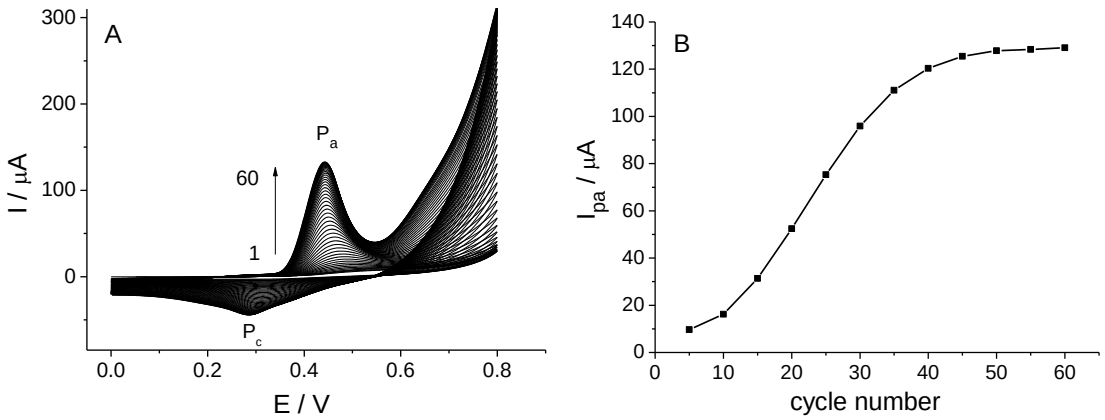

Figure 1. (A) Consecutive cyclic voltammograms of NiHCF/CPE in 1 M NaOH solution. Scan rate: 0.1 V s^{-1}. (B) Plot of I_{pa} vs. cycle number.

The nickel hydroxide was prepared by a facile in situ electrochemical method. Fig. 1A shows the consecutive cyclic voltammograms of NiHCF/CPE in 1 M NaOH solution. As shown, on the first cycle, an anodic peak P_a at + 0.52 V and a cathodic peak P_c at + 0.34 V corresponding to the redox of NiHCF were observed [24]. On the second and subsequent cycles, the peak potential of P_a and P_c shifted to the

negative direction, and finally stayed at 0.45 V and 0.29 V respectively. Meanwhile, the peak currents of P_a and P_c increased gradually and became constant after 45 cycles (Fig. 1B), indicates that NiHCF has converted to $Ni(OH)_2$ completely [16, 25, 35].

3.2. Characterization of nickel hydroxide flakes

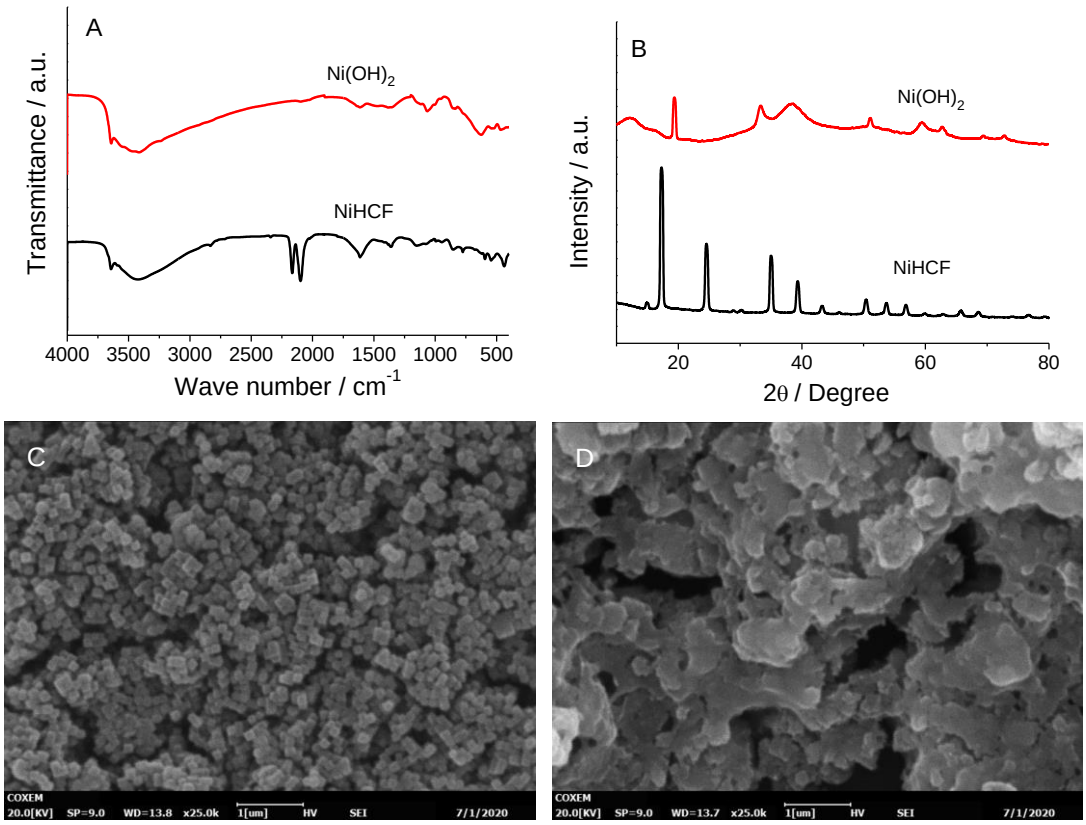

Figure 2. (A) FTIR spectra, (B) XRD spectra, and SEM images of (C) NiHCF and (D) $Ni(OH)_2$.

Fig. 2A shows the FTIR spectra of NiHCF and $Ni(OH)_2$. For NiHCF, the typical absorption peaks at 2181 and 2094 cm^{-1} assigned to *v* (−CN) in the lattice of FeIII/II-CN-NiII. While for $Ni(OH)_2$, the *v* (−CN) disappeared. The characteristic vibration at 3641, 3415, and 530 cm^{-1} were due to *v* (free −OH), *v* (−OH), and *v* (Ni−OH), respectively [28].

Fig. 2B shows the powder XRD spectra of NiHCF and $Ni(OH)_2$. For NiHCF, the sharp diffraction peaks at 15°, 17°, 24°, 36°, 39°, 43°, 51°, 54°, 57°, 66°, 68° correspond to the diffraction planes of (111), (200), (220), (400), (420), (422), (440), (600), (620), (640) and (642) of NiHCF (JCPDS No.00-051-1897), indicate the good crystalline particles and the successfully prepared of NiHCF complex. For the electrochemically synthesized $Ni(OH)_2$, the characteristic diffraction peaks at 19.3°, 33.1°, 38.5°, 52.1°, 59.1°, 62.7°, 69.4° and 72.8° correspond to the diffraction planes of (001), (100), (101), (102), (110), (111), (200) and (201) of crystalline β-$Ni(OH)_2$ (JCPDS No.00-014-0117), and no other diffraction peaks observed, confirm the formation of pure phase crystalline β-$Ni(OH)_2$.

Furthermore, the morphology of the resulting products has characterized by SEM. As shown in Fig. 2C, the NiHCF consists of 3D cubic structures with an average size of 100 nm. The NiHCF derived

$Ni(OH)_2$ becomes hierarchical 2D flake structures with the size range of 0.1~1μm. Predictably, this hierarchical flake structure would have a large surface area and increase the sensitivity of the sensor.

3.3. Electrochemical characterization of $Ni(OH)_2$/CPE

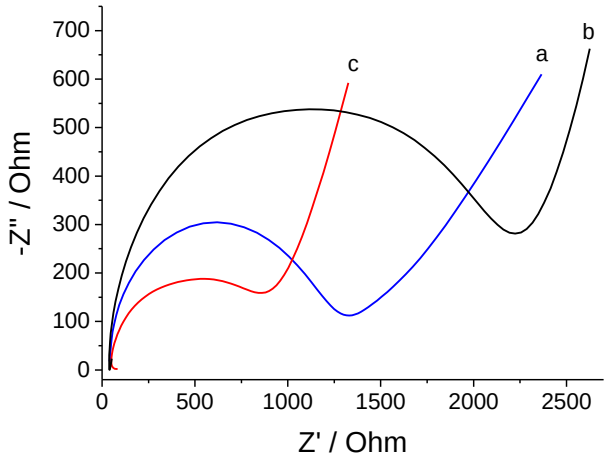

Figure 3. Nyquist diagrams of CPE (a), NiHCF/CPE (b), and $Ni(OH)_2$/CPE in 0.1 M KCl solution containing 5.0 mM $[Fe(CN)_6]^{3-/4-}$, frequency for EIS: 0.1 Hz to 100.0 kHz.

The electrochemical characterization of $Ni(OH)_2$/CPE was carried out by electrochemical impedance spectroscopy (EIS) in 0.1 M KCl solution containing 5.0 mM $[Fe(CN)_6]^{3-/4-}$. Commonly, the electron transfer resistance (R_{ct}) which equal to the diameter of the semicircle reveals the electron transfer efficiency of the redox molecules at the electrode surface. Fig. 3 shows the Nyquist diagrams of different electrodes. As shown, the diameters of semicircle observed are in the sequence of $Ni(OH)_2$/CPE<CPE< NiHCF/CPE, suggests that the interfacial R_{ct} at $Ni(OH)_2$/CPE is smallest, and the electron transfer efficiency at $Ni(OH)_2$/CPE is higher than that at CPE and NiHCF/CPE. Thus, $Ni(OH)_2$/CPE will be a good platform for sensing applications.

Moreover, chronocoulometry was conducted to investigate the active surface areas of CPE, NiHCF/CPE and $Ni(OH)_2$/CPE. Fig. 4A shows the *Q*–*t* curves of the electrodes in 1.0 M KCl solution containing 0.1 mM $K_3[Fe(CN)_6]$. Based on Anson's equation [38]:

$$Q\,(t) = (2nFAcD^{1/2}t^{1/2}) / \pi^{1/2} + Q_{dl} + Q_{ads} \quad (1)$$

The active surface area A of the working electrode can be estimated by the slope of the plot $Q - t^{1/2}$. Since the slope of the plot Q–$t^{1/2}$ for CPE, NiHCF/CPE, and $Ni(OH)_2$/CPE are 2.275, 7.512, and 18.91 (Fig. 4B), the active surface area of CPE, NiHCF/CPE and $Ni(OH)_2$/CPE are 0.0859, 0.2838, and 0.7143 cm^2, respectively (D = 7.6×10^{-6} $cm^2\ s^{-1}$). The larger surface area of $Ni(OH)_2$/CPE attributes to the hierarchical flake structure of $Ni(OH)_2$, which would supply more active sites for hydrazine sensing and lead to high electrochemical reactivity.

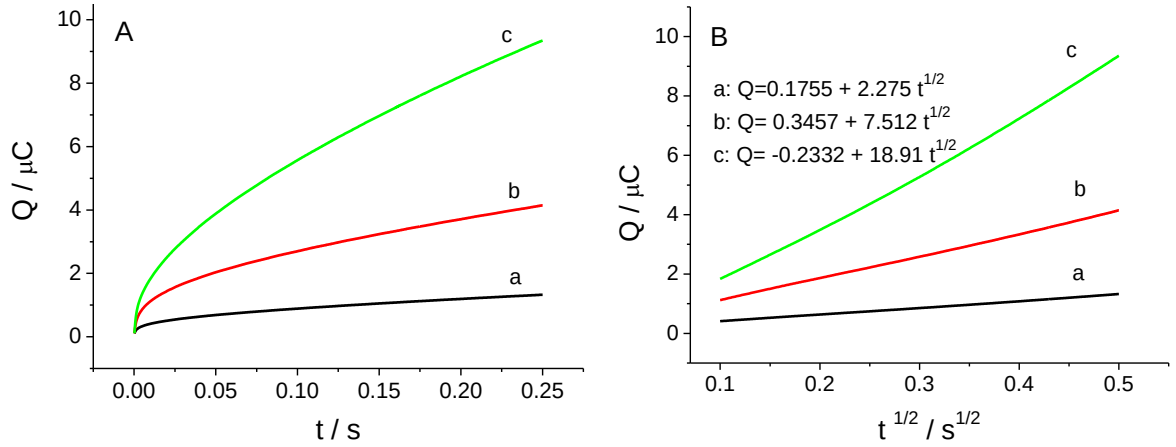

Figure 4. (A) Plot of Q–t curves, and (B) Plot of Q–$t^{1/2}$ curves of CPE (a), NiHCF/CPE (b), and $Ni(OH)_2$/CPE (c) in 1.0 M KCl containing 0.1 mM $K_3[Fe(CN)_6]$.

3.4. Electrocatalytic oxidation of hydrazine at $Ni(OH)_2$/CPE

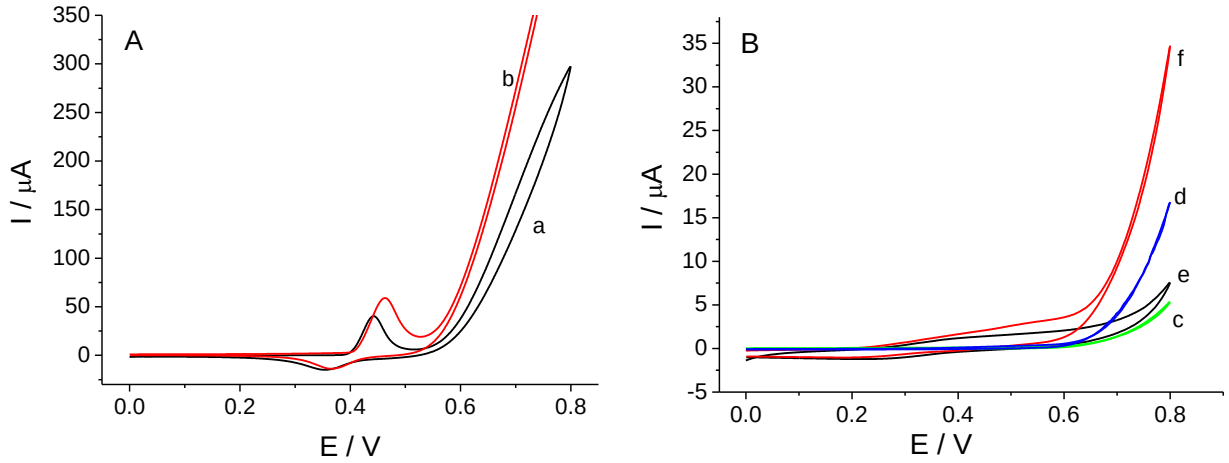

Figure 5. Cyclic voltammograms of (A) $Ni(OH)_2$/CPE, (B) CPE and NiHCF/CPE in the absence (a, c, d) and presence (b, d, f) of 20 μM hydrazine in 0.1 M NaOH solution. Scan rate: 20 mVs^{-1}.

The performance of $Ni(OH)_2$/CPE to the electrochemical oxidation of hydrazine were evaluated by cyclic voltammetry. Fig. 5 shows the cyclic voltammograms at $Ni(OH)_2$/CPE, CPE, and NiHCF/CPE in the absence and the presence of hydrazine. As shown, in the absence of hydrazine, a pair of redox peaks correspond to the Ni(III)/Ni(II) couple are observed at $Ni(OH)_2$/CPE [16, 25, 35] (Fig. 5A, curve a). However, in the presence of hydrazine (Fig. 5A, curve b), the anodic peak corresponds to the oxidation of Ni(II) to Ni (III) increases obviously with the peak current of 17.81 μA. At the reverse scan, the cathodic peak corresponds to the reduction of Ni(III) to Ni(II) decreases slightly. This fact indicates that $Ni(OH)_2$/CPE has a catalytic effect on the hydrazine oxidation. Meanwhile, the oxidation of hydrazine at CPE has an increase in the background current but no anodic peak appears (Fig. 5B, curve c, d). The peak current of the electro-oxidation of hydrazine at NiHCF/CPE is 2.18 μA (Fig. 5B, curve e, f), which is lower than that at $Ni(OH)_2$/CPE. These results indicate that the β-$Ni(OH)_2$ flakes can improve the performance of hydrazine oxidation.

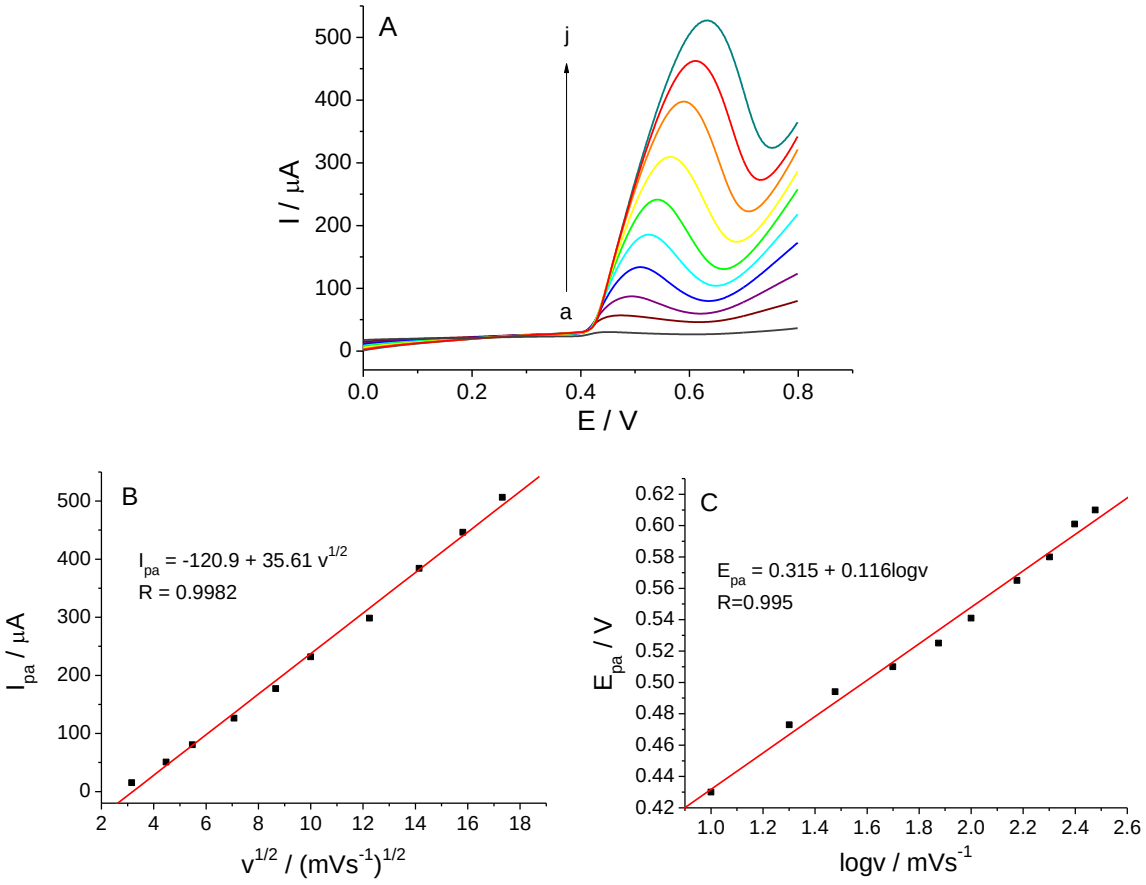

Figure 6. (A) Linear sweep voltammograms of $Ni(OH)_2$/CPE in 0.1 M NaOH solution containing 20 μM hydrazine at scan rate of (from a to j) 10, 20, 30, 50, 75, 100, 150, 200, 250, 300 mVs^{-1}. (B) Plot of I_{pa} vs. $v^{1/2}$. (C) Plot of E_{pa} vs. log$v$.

Furthermore, the oxidation current of hydrazine is proportional to the square root of scan rate v (Fig. 6A, 6B), which indicates that the electro-catalytic process of hydrazine is diffusion-controlled and depends on the hydrazine concentration in solution. Moreover, the oxidation peak potential of hydrazine shows a positive shift with the increase of scan rate v (Fig. 6A, 6C). Based on the Laviron equation [39]:

$$E_{pa} = E° + \left(\frac{2.303RT}{\alpha nF}\right)\log\left(\frac{RTk°}{\alpha nF}\right) + \left(\frac{2.303RT}{\alpha nF}\right)\log v \quad (2)$$

From the slope of the relationship between E_{pa} vs. log$v$, the number of electrons transferred in the rate-determining step of hydrazine oxidation was calculated to be 1. Thus, the electro-catalytic oxidation process of hydrazine at $Ni(OH)_2$/CPE can express as follows [16, 35]:

$N_2H_4 + OH^- \rightarrow N_2H_3 + H_2O + e^-$ (slow) (3)

$N_2H_3 + 3OH^- \rightarrow N_2 + 3H_2O + 3e^-$ (fast) (4)

$N_2H_4 + 4OH^- = N_2 + 4H_2O + 4e^-$ (overall reaction) (5)

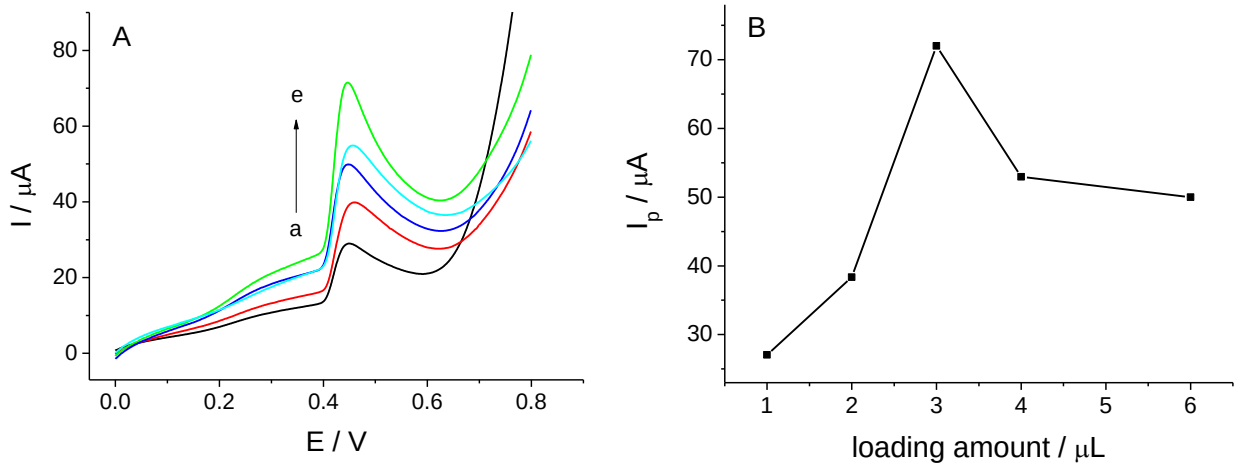

Figure 7. (A) Linear sweep voltammograms of $Ni(OH)_2$/CPE in 0.1 M NaOH containing 20 μM hydrazine, loading amount of NiHCF from a to e: 1, 2, 4, 5, 3 μL, scan rate: 20 mV s^{-1}. (B) Plot of I_p vs. loading amount of NiHCF.

3.5. Optimization of loading amount of NiHCF

To get the optimum responses of $Ni(OH)_2$/CPE to the electro-catalytic oxidation of hydrazine, the loading amount of NiHCF on the peak current I_p of hydrazine were investigated. As shown in Fig. 7, when the loading amount of NiHCF increases from 1 to 3 μL, the oxidation peak currents of hydrazine enhance obviously, which might attribute to the increase of the electron transfer efficiency of $Ni(OH)_2$/CPE by the improve amount of NiHCF. However, further improves the NiHCF amount results in the decrease of oxidation peak currents. In consequence, 3 μL of NiHCF is the optimum content for the preparation of $Ni(OH)_2$/CPE.

3.6. Quantification of hydrazine

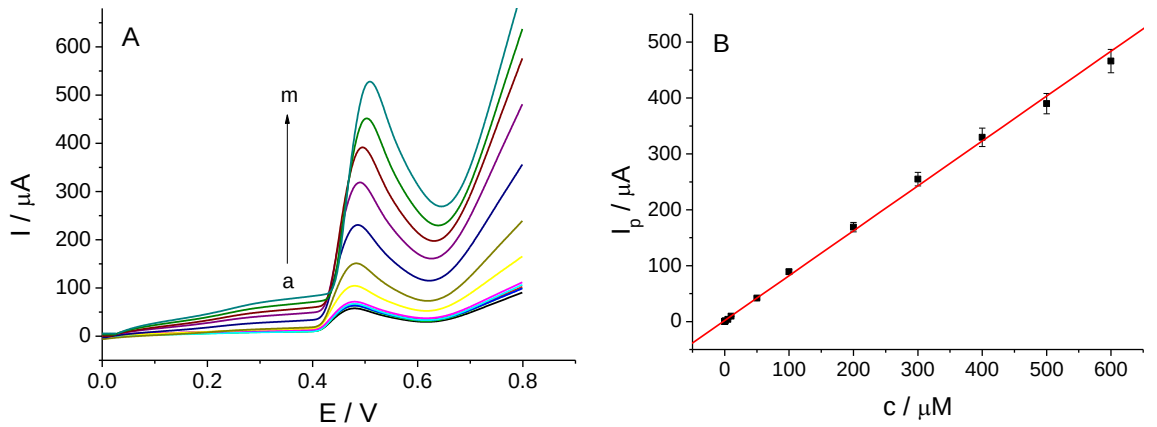

Figure 8. (A) Linear sweep voltammograms of hydrazine at $Ni(OH)_2$/CPE in 0.1 M NaOH solution. The concentration of hydrazine from a to m: 0, 0.1, 0.5, 1, 5, 10, 50, 100, 200, 300, 400, 500, 600 μM. (B) Plot of I_p vs. c.

Fig. 8 shows the linear sweep voltammograms (LSV) of hydrazine at $Ni(OH)_2$/CPE under optimized experimental conditions. As shown, the response current increases gradually with the increase of hydrazine concentration and is linear with the hydrazine concentration in the range of 0.1 to 600 μM. The linear regression equations is I (μA) = 1.651 + 0.8035 c (μM) (R = 0.9992), the limit of detection is 0.04 μM (3S/N). Table 1 shows the comparison of the analytical performances of $Ni(OH)_2$/CPE with those literature reports.

Table 1. Comparison of analytical performances of some electrochemical sensors for hydrazine

Working Electrode	Linear Range (μM)	Detection Limit (μM)	Sensitivity (μA mM^{-1})	Reference
FeCo oxide-carbon spheres / GCE	0.1–516.6	0.1	123	8
CuNS-MWCNT / PGE	0.1–800	0.07	635.9	9
ZnO NPs/PEDOT:PSS	10–500	5	140	7
f–MWCNTs/pTBO/GCE	1–357	0.24	2492	13
Ni(II)–BA–MWCNT–PE	2.5–200	0.8	69.9	16
NiFeHCF / CPE	0.5–2000	0.05	132.83	24
$Ni(OH)_2$ nanoplates / Cu rod	1–15931	0.3	111.6	34
$Ni(OH)_2$ nanoplatelets / CPE	1−1300	0.28	1330	35
$Ni(OH)_2$–MnO_2 / GCE	5–18000	0.12	25	36
β-$Ni(OH)_2$ flakes /CPE	0.1−600	0.04	803.5	This work

3.7. Interference studies

The influence of some substances on the quantification of hydrazine was evaluated. As shown in Fig. 9, the relative deviations of 100-fold of K^+, NH_4^+, Ca^{2+}, Mg^{2+}, Fe^{2+}, Zn^{2+}, Cl^-, Ac^-, CO_3^{2-}, and SO_4^{2-} on the determination are less than 5%, indicating the good selectivity of the method.

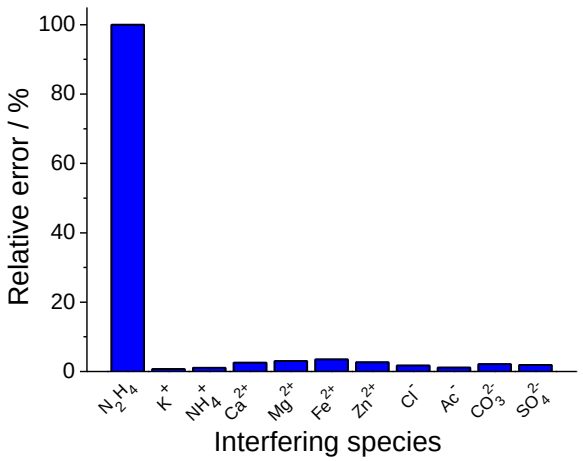

Figure 9. Relative error of current response of $Ni(OH)_2$/CPE to the addition of 20 μM hydrazine and 100-fold of different interfering species.

3.8. Repeatability, reproducibility and stability

The relative standard deviation (RSD) for ten replicate measurements of 10 μM hydrazine was 3.1%. The RSD of five pieces of $Ni(OH)_2$/CPE with the same surface area for the determination of 10 μM hydrazine was 3.7 %. After 30 days of storage at room temperature, the current response of $Ni(OH)_2$/CPE for 10 μM hydrazine was 96.2% of the original value. These results prove that the $Ni(OH)_2$/CPE has good repeatability, reproducibility and stability for hydrazine measurement.

3.9. Analytical application

The proposed method was applied to monitoring the hydrazine concentration in water samples by the standard addition method. As shown in Table 2, the measured recoveries are in the range of 98.3% ~ 105%, indicating that the $Ni(OH)_2$/CPE is promising for the quantification of hydrazine.

Table 2. Quantification results of hydrazine in water samples

Sample (River water)	Hydrazine added (μM)	Hydrazine found (μM)*	Recovery (%)
1	0	_	_
2	5	5.25	105
3	50	50.9	102
4	100	98.3	98.3

*Average of five measurements ± RSD

4. CONCLUSIONS

A β-$Ni(OH)_2$ flakes modified carbon paste electrode $Ni(OH)_2$/CPE for hydrazine sensing was fabricated. The β-$Ni(OH)_2$ flakes synthesized from NiHCF nanocubes by a facile in situ electrochemical method. The high surface area and the excellent electron transfer efficiency of hierarchical β-$Ni(OH)_2$ flakes enhanced the oxidation peak current of hydrazine. Moreover, the sensor exhibited low detection limit, high sensitivity, good stability and reproducibility.

ACKNOWLEDGEMENT
The authors thank the financial support from the Science & Technology Foundation of Xi'an Shiyou University (Z09137) and University Student Innovation Fund of Xi'an Shiyou University (2019). Thank the instruments support from Modern Analysis &Test Center of Xi'an Shiyou University [Nicolet 5700 FTIR spectrometer (Thermo) and D8 X-ray polycrystalline diffractometer (Bruker)].

References

1. H. Hamidi, S. Bozorgzadeh, B. Haghighi, *Microchim. Acta,* 184 (2017) 4537.
2. G. Choudhary, H. Hansen, *Chemosphere,* 37 (1998) 801.
3. S. Garrod, M.E. Bollard, A.W. Nicholls, S.C. Connor, J. Connelly, J.K. Nicholson, E. Holmes,

Chem. Res. Toxicol., 18 (2005) 115.
4. J.A. Oh, H.S. Shin, *Anal. Chim. Acta,* 950 (2017) 57.
5. S.K. Manna, *ChemistrySelect,* 4 (2019) 7219.
6. J. Liu, J. Jiang, Y. Dou, F. Zhang, X. Liu, J. Qua, Q. Zhu, *Org. Biomol. Chem.,* 17 (2019) 6975.
7. T. Beduk, E. Bihar, S.G. Surya, A.N. Castillo, S. Inal, K.N. Salama, *Sens. Actuators B,* 306 (2020) 127539.
8. D.M. Nguyen, L.G. Bach, Q.B. Bui, *J. Pharm. Biomed. Anal.,* 172 (2019) 243.
9. H. Heydari, M.B. Gholivand, A. Abdolmaleki, *Mater. Sci. Eng. C,* 66 (2016) 16.
10. R. Ahmad, N. Tripathy, M.S. Ahn, Y.B. Hahn, *J. Colloid Interface Sci.,* 494 (2017) 153.
11. K.P. Sambasevam, S. Mohamad, S.W. Phang, *J. Appl. Polym. Sci.,* 132 (2015) 41746.
12. M.R. Majidi, A. Jouyban, K. Asadpour-Zeynali, *Electrochim. Acta,* 52 (2007) 6248.
13. B. Sriram, T.W. Chen, S.M. Chen, K.K. Rani, R. Devasenathipathy, S.F. Wang, *Int. J. Electrochem. Sci.,* 13 (2018) 4901.
14. S. Cao, S. Zheng, H. Pang, *Microchim. Acta,* 187 (2020)168.
15. M. Nemakal, S. Aralekallu, I. Mohammed, S. Swamy, L.K. Sannegowda, *J. Electroanal. Chem.,* 839 (2019) 238.
16. L. Zheng, J. Song, *Talanta,* 79 (2009) 319.
17. W. Li, B. Zhang, R. Lin, S. Ho-Kimura, G. He, X. Zhou, J. Hu, I. P. Parkin, *Adv. Funct. Mater.,* 28 (2018) 1705937.
18. Y. Yuan, D. Bin, X. Dong, Y. Wang, C. Wang, Y. Xia, *ACS Sustainable Chem. Eng.,* 8 (2020) 3655.
19. L. Zhang, D. Shi, T. Liu, M. Jaroniec, J. Yu, *Mater. Today,* 25 (2019) 35.
20. R.S. Kate, S.A. Khalate, R.J. Deokate, *J. Alloy Compd.,* 734 (2018) 89.
21. A. QayoomMugheri, A.Tahira, U. Aftab, M. IshaqAbro, S.R. Chaudhry, L. Amaral, Z.H. Ibupoto, *Electrochim. Acta,* 306 (2019) 9.
22. L. Zheng, C. He, *J. Solid State Electrochem.,* 23 (2019) 2595.
23. G. Başkaya, Y. Yıldız, A. Savk, T.O. Okyay, S. Eriş, H. Sert, F. Şen, *Biosens. Bioelectron.,* 91 (2017) 728.
24. P.C. Pandey, D. Panday, *J. Electroanal. Chem.,* 763 (2016) 63.
25. L. Zheng, W. Zhang, J. Guo, *Ionics,* 26 (2020) 449.
26. H.B. Li, M.H. Yu, F.X. Wang, P Liu, Y Liang, J Xiao, C.X. Wang, Y.X. Tong, G.W. Yang, *Nat. Commun.,* 4 (2013) 1894.
27. V. Lakshmi, R. Ranjusha, S. Vineeth, S.V. Nair, A. Balakrishnan, *Colloids Surf. A,* 457 (2014) 462.
28. S. Kaipannan, S. Marappan, *Sci. Rep.,* 9 (2019)1104.
29. R. Wang, A. Jayakumar, C. Xu, J.M. Lee, *ACS Sustainable Chem. Eng.,* 4 (2016) 3736.
30. X. Zhu, Y. Zhong, H. Zhai, Z. Yan, D. Li, *Electrochim. Acta,* 132 (2014) 364.
31. Z. Xing, L. Gan, J. Wang, X. Yang, *J. Mater. Chem. A,* 5 (2017) 7744.
32. D. Wang, W. Yan, S.H. Vijapur, G.G. Botte, *J. Power Sources,* 217 (2012) 498.
33. H. Heli, N. Sattarahmady, R.D. Vais, K. Karimian, *Sens. Actuators B,* 196 (2014) 631.
34. R. Ji, Y. Huang, L. Wang, L. Yu, J. Wang, G. Wang, X. Zhang, *Mater. Res. Bull.,* 48 (2013) 3729.
35. A. Avanes, M. Hasanzadeh-Karamjavan, G. Shokri-Jarcheloo1, *Microchim. Acta,* 186 (2019) 441.
36. M.U.A. Prathap, V. Anuraj, B. Satpati, R. Srivastava, *J. Hazard. Mater.,* 262 (2013) 766.
37. Y. Liu, Y. Qiao, W. Zhang, Z. Li, X. Ji, L. Miao, L. Yuan, X. Hu, Y. Huang. *Nano Energy,* 12 (2015) 386.
38. F.C. Anson, *Anal. Chem.,* 36 (1964) 932.
39. E. Laviron, *J. Electroanal. Chem.,* 101 (1979) 19.